



PCCP

Bandgap widening through doping for improving the photocatalytic oxidation ability of narrow-gap semiconductors

Journal:	<i>Physical Chemistry Chemical Physics</i>
Manuscript ID	CP-ART-07-2022-002994.R2
Article Type:	Paper
Date Submitted by the Author:	02-Nov-2022
Complete List of Authors:	<p>Yang, Yue; Tokyo Institute of Technology, School of Materials and Chemical Technology Toyoda, Masayuki; Tokyo Institute of Technology, Department of Physics Yamaguchi, Akira; Tokyo Kogyo Daigaku, Cho, Yohei; Tokyo Institute of Technology, Department of Materials Science and Engineering; Tokyo Institute of Technology, Department of Materials Science and Engineering Aisnada, An Niza El; Tokyo Institute of Technology Abe, Hideki; National Institute for Materials Science, Hydrogen Production UEDA, Shigenori; National Institute for Materials Science, Synchrotron X-ray Group; National Institute for Materials Science, Okunaka, Sayuri; National Institute of Advanced Industrial Science and Technology Tsukuba West, ; Saito, Susumu; Tokyo Institute of Technology, Advanced Research Center for Quantum Physics and Nanoscience Liu, Min; Central South University, Department of Physics Tokudome, Hiromasa; TOTO Ltd Miyauchi, Masahiro; Tokyo Institute of Technology, Graduate School of Science and Engineering</p>

ARTICLE

Bandgap widening through doping for improving the photocatalytic oxidation ability of narrow-gap semiconductors

Yue Yang,^a Masayuki Toyoda,^b Akira Yamaguchi,^a Yohei Cho,^a An Niza El Aisnada,^a Hideki Abe,^c Shigenori Ueda,^{d,e,f} Sayuri Okunaka,^g Susumu Saito,^{b,h,i} Min Liu,^j Hiromasa Tokudome^{k,*}, Masahiro Miyauchi^{a,*}

Received 00th January 20xx,
Accepted 00th January 20xx

DOI: 10.1039/x0xx00000x

The trade-off relationship between narrowing the bandgap and achieving sufficient redox potentials accounts for the hindrance to the development of an efficient photocatalyst. Most previous researchers attempt to narrow the bandgap of semiconductors by impurity doping to achieve visible-light sensitivity, but this approach causes the losses of their oxidation and/or reduction powers. Conversely, this study presents a bandgap widening strategy by doping to improve the redox potential of photogenerated carriers. Employing first-principles simulations, we propose the lanthanum-doped bismuth vanadate (La-BiVO₄) photocatalyst as a wider-bandgap semiconductor exhibiting stronger oxidation power compared to pristine BiVO₄, and the results revealed that the bismuth orbital in the valence band (VB) was diluted by lanthanum-ion doping, while VB shifted to a higher potential (positively shifted). Thereafter, an La-BiVO₄ powder was synthesized via a solid-state reaction, after which its activity was evaluated in the photocatalytic oxidation of 2-propanol (IPA). La-BiVO₄ exhibited bandgap widening; thus, the number of absorbed photons under visible-light irradiation was lower than that with pristine BiVO₄. However, the quantum efficiency (QE) of La-BiVO₄ for the oxidation of IPA was higher than that of the pristine BiVO₄. Consequently, the photocatalytic reaction rate of La-BiVO₄ was superior to that of pristine BiVO₄ under the same visible-light irradiation conditions. Although the bandgap of La-BiVO₄ is widened, it is still sensitive to the cyan-light region, which is the strongest in the sunlight spectrum. These results demonstrate that the orbital dilution strategy by impurity elemental doping is effective for bandgap widening and contributes to improving the oxidation and/or reduction powers of the photogenerated charge carriers. This study elucidates the possibility of boosting photocatalytic performances via bandgap widening.

1. Introduction

Photocatalysts have been extensively studied for their potential utility on solving environmental and energy

problems.¹ The photocatalytic process involves two main steps: the first one comprises the absorption of light to excite electrons from the valence band (VB) to the conduction band (CB), and the second step involves the migration of the excited charge carriers to the surface of the catalysts, as well as their participation in chemical reactions. The trade-off relationship between the narrow bandgap (for absorbing more solar light) and the sufficient redox potentials of CB and VB in chemical reactions accounts for the hindrance to the development of an efficient photocatalyst. For instance, titanium dioxide (TiO₂), which has been widely reported in photocatalytic energy conversions and environmental purification, exhibits a bandgap value of 3.2 eV² and could drive different oxidation and reduction reactions^{3, 4}. However, TiO₂ can only absorb light exhibiting a wavelength that is shorter than 380 nm, which is <5% of solar energy.

A method for enhancing the solar-energy-utilization efficiency involves the sensitization of the wide-gap semiconductors into visible-light-responsive ones via doping. For example, nitrogen-doped TiO₂ exhibited an external quantum efficiency (EQE) of 0.42% under blue-light irradiation (<436 nm), while that of pristine TiO₂ was only 0.14%². However, doping hampers the photocatalytic performance of the photocatalyst because of the

^a Department of Materials Science and Engineering, School of Materials and Chemical Technology, Tokyo Institute of Technology, 2-12-1 Ookayama, Meguro, Tokyo 152-8552, Japan.

^b Department of Physics, School of Science, Tokyo Institute of Technology, 2-12-1 Ookayama, Meguro, Tokyo 152-8551, Japan.

^c Center for Green Research on Energy and Environmental Materials, National Institute for Materials Science, 1-1, Namiki, Tsukuba, Ibaraki 305-0044, Japan.

^d Synchrotron X-ray Station at SPring-8, National Institute for Materials Science, 1-1-1 Kouto, Sayo, Hyogo 679-5148, Japan.

^e Research Center for Advanced Measurement and Characterization, National Institute for Materials Science, 1-2-1 Sengen, Tsukuba, Ibaraki 305-0047, Japan.

^f Research Center for Functional Materials, National Institute for Materials Science, 1-1 Namiki, Tsukuba, Ibaraki 305-0044, Japan.

^g Global Zero Emission Research Center (GZR), National Institute of Advanced Industrial Science and Technology (AIST), 16-1 Onogawa, Tsukuba, Ibaraki, 305-8559, Japan.

^h Advanced Research Center for Quantum Physics and Nanoscience, Tokyo Institute of Technology, 2-12-1 Ookayama, Meguro-ku, Tokyo 152-8551, Japan.

ⁱ Materials Research Center for Element Strategy, Tokyo Institute of Technology, 4259 Nagatsuta-cho, Midori-ku, Yokohama, Kanagawa 226-8503, Japan.

^j Hunan Joint International Research Center for Carbon Dioxide Resource Utilization, School of Physical and Electronics, Central South University, Changsha, Public Republic of China.

^k Research Institute, TOTO Ltd, 2-8-2 Honson, Chigasaki, Kanagawa 253-8577, Japan.

Electronic Supplementary Information (ESI) available: See DOI: 10.1039/x0xx00000x

limited redox potential of doped states⁵, and these dopants function as recombination centers for electron–hole pairs. In addition to these studies, different intrinsic semiconductors with suitable bandgap values and band positions have been investigated as photocatalysts⁶. However, these photocatalysts could not still satisfactorily solve the trade-off relationship because of the limited choice of pristine photocatalysts for driving the expected redox reactions. Thus, methods other than bandgap narrowing are being explored to break the bottleneck of photocatalyst development.

Compared with the sensitization of visible-light responsiveness via bandgap narrowing, fewer studies have focused on stimulating the photocatalytic activity of intrinsic narrow-gap semiconductors via bandgap widening. For example, it has been reported that indium and molybdenum dual-doped multiphase bismuth vanadate (BiVO_4) exhibits a 0.07 eV wider bandgap and a 0.15 V negatively shifted CB potential⁷. In addition to tuning the CB position, VB tuning is more vital, especially for improving the oxidation power during the decomposition of organic contaminants. Indeed, Yu et al. tuned the VB of Cu_2O via halogen doping, and the VB position was 0.34 V positively shifted⁸. However, self-oxidation occurs in Cu_2O because the VB top comprises halogen orbitals.

BiVO_4 is a widely known excellent visible-light-responsive photocatalyst that can drive water oxidation reactions. However, its applications in photocatalytic organic oxidation have been less reported than those of TiO_2 or WO_3 because of its insufficient oxidation power^{9,10}. Unfortunately, TiO_2 and WO_3 are only responsive to the ultraviolet (UV) and blue-light regions. Contrarily, BiVO_4 can absorb green-cyan light (500–550 nm), which exhibits the strongest intensity in the solar spectrum. Here, we selected BiVO_4 to demonstrate bandgap widening by tuning its VB position via doping. We expected that BiVO_4 exhibiting a widened bandgap would improve the photocatalytic oxidation power while remaining responsive to the cyan light. The lone pairs of electrons in scheelite monoclinic BiVO_4 formed unique VB comprising hybrid Bi 6s and O 2p orbitals^{11, 12}. These metal s and oxygen p hybridized orbitals lifted the VB position upward compared to those formed by only the O 2p orbitals¹³. Thus, exploiting this special property, we proposed the tuning of VB of BiVO_4 through an orbital dilution strategy. To dilute the bismuth orbital contribution into VB and maintain the scheelite monoclinic structure, we selected lanthanum to substitute the bismuth site. Although previous researches have investigated similar La doped BiVO_4 systems^{14, 15}, they didn't give a sophisticated discussion regarding band structure change and the succeeding impacts on photocatalytic performance with a varying La doping level. Lanthanum ions was chosen since that the trivalent lanthanum ions had the closest ionic radius to that of trivalent bismuth ions. More importantly, the orbital of the La^{3+} did not overlap in the forbidden gap between O 2p and the metal d-orbital¹⁶.

First, we conducted first-principles calculations to confirm the rationality of the proposed bandgap widening strategy.

Subsequently, we experimentally synthesized La-doped BiVO_4 and characterized its different properties. Further, its photocatalytic activity in the oxidation of 2-propanol (IPA) into acetone was evaluated. We compared the different factors, including the absorbed photon numbers, QE, surface area, crystallinity, gas adsorption properties, and photocatalytic oxidation reaction rates, that affected the photocatalytic performances of La-doped and pristine BiVO_4 . Here, the concept of bandgap widening to improve oxidation activity was elucidated by first-principles calculations and experimental studies.

2. Methodology

2.1 First-principles calculations

The Vienna Ab initio Simulation Package (VASP) code was utilized for the first-principles calculations^{17,18,19,20} employing the frozen-core projector-augmented wave method^{21,22}. The exchange-correlation functional was described by the Perdew–Burke–Ernzerhof (PBE) functional within the generalized gradient approximation (GGA)^{23,24}, and the cutoff energy was set to 600 eV. BiVO_4 exhibited a scheelite monoclinic structure (space group and number are C2/c and 15, respectively) as its crystal structure, and the atomic coordination and lattice constant parameters were obtained from the experimental result²⁵. In the calculations, a $2a \times b \times 2c$ supercell comprising 16, 16, and 64 bismuth, vanadium, and oxygen atoms, respectively, was employed to prevent the self-interactions of the dopant along each direction. The k-point mesh of the 96-atom supercell structure was $2 \times 2 \times 3$. The model of the La-doped BiVO_4 structure was constructed by replacing the bismuth atom with the lanthanum one. To investigate the influence of the doping amount, three structure models exhibiting different doping levels were constructed, as follows: 0 at%, 6.25 at% (one La atom of 16 Bi sites), and 12.5 at% (two La atoms of 16 Bi sites). Regarding the 12.5 at% La-doped BiVO_4 , two Bi atoms need to be substituted, and the relative position of these two dopants was considered. Here, we selected the two most distant bismuth sites for lanthanum-atom doping to investigate the orbital dilution strategy. The other doping pattern choices are reported in the Supporting Information (SI Note 1, Figure S1, and Table S1).

The ionic relaxation step was performed to thoroughly relax the residual force in each input structure. We adapted the conjugate gradient method to fully relax all the atoms with a break condition of 1×10^{-3} eV. Considering the possible distortion of the crystal symmetry generally caused by doping, we removed the symmetry constraint during the ionic relaxation step²⁶. The parameters of the optimized structures are listed in Table S2. Subsequently, these optimized structures were adapted for further density-of-states (DOS) calculations.

2.2 Materials synthesis

We synthesized the La-doped BiVO₄ via a solid-state reaction. Commercial metal oxides, *i.e.*, La₂O₃, Bi₂O₃, and V₂O₅ (Wako Chemicals), were employed as precursors for the synthesis. Owing to the reactivity of La₂O₃ with water and carbon dioxide²⁷, the obtained La₂O₃ powder was heated for 1 h at 700 °C before each weighing to guarantee a precise doping ratio. We weighed the La₂O₃ powder after cooling it to 150 °C. Additionally, only the La₂O₃ powder was subjected to this pretreatment. Rather, Bi₂O₃ and V₂O₅ were stable during storage. The Bi₂O₃, La₂O₃, and V₂O₅ chemicals were weighed in proportions and mixed employing a planetary ball-milling machine for 2 h at 200 rpm. Ethanol was added as a milling medium. After the ball-milling process, the mixtures were collected and calcined in a muffle furnace for 5 h at 600 °C with a heating rate of 5 °C/min. Subsequently, the heated chemicals were thoroughly mixed in a mortar and calcined for 2 h at 800 °C.

We varied the ratios of the raw materials to investigate the influence of the lanthanum doping concentration. In a typical synthesis process, 4.66 and 1.82 g of Bi₂O₃ and V₂O₅, respectively, were employed to prepare pristine BiVO₄; 4.43, 0.16, and 1.82 g of Bi₂O₃, La₂O₃, and V₂O₅, respectively, were employed to prepare 5 at% La–BiVO₄; 4.19, 0.33, and 1.82 g of Bi₂O₃, La₂O₃, and V₂O₅, respectively, were employed to prepare 10 at% La–BiVO₄; and 3.96, 0.50, and 1.82 g of Bi₂O₃, La₂O₃, and V₂O₅, respectively, were employed to prepare 15 at% La–BiVO₄.

2.3 Material characterization

The crystal structure was measured via X-ray diffraction (XRD, Rigaku SmartLab diffractometer equipped with a D/teX ultra-detector) in the 2θ range of 3°–90°. For the elemental mapping, energy-dispersive X-ray spectroscopy (EDS) was performed on a JEOL JEM-2010F transmission electron microscope. The UV–visible (Vis) spectra were recorded on a JASCO V-670 spectrometer employing an integration sphere unit (the diffuse reflectance method) in the wavelength range of 300–800 nm employing BaSO₄ for the baseline calibration. Photoluminescence (PL) spectra were measured using a fluorescence spectrophotometer (F-7000, Hitachi, Japan) with 355 nm excitation light. Inductively coupled plasma mass spectrometry (ICP-MS) analysis was performed to measure the chemical composition of the La-to-Bi ratio. Hard X-ray photoelectron spectroscopy (HAXPES) was performed at the undulator beamline BL15XU of SPring-8. Thermogravimetric and differential thermal analyses coupled with mass spectrometry (TG–DTA, NETZSCH, STA2500 Regulus) were performed to analyze the gaseous IPA and acetone adsorption properties at 25 °C. Initially, pure N₂ was purged for 20 min to obtain a clean material surface. Subsequently, acetone (or IPA) was purged with the carrier gas. Detailedly, the carrier gas (N₂) was purged into liquid acetone (or IPA), after which a mixture of the gas and acetone (or IPA) was continuously purged into the chamber for 5 min. The mass difference of this process was determined.

2.4 Evaluation of photocatalytic activity

The oxidation of IPA into acetone was selected to evaluate the photocatalytic activity because of its simple and clear reaction route (SI Note 2)²⁸. In this experiment, we employed a photoacoustic multi-gas monitor (INNOVA AirTech Instrument A/S) to measure the changes in the concentrations of IPA and acetone. Next, 0.2 g of the photocatalyst powder was evenly dispersed on a glass Petri dish (5.5 cm²) employing water as the agent; the water was evaporated via heating on a hot plate (90 °C). The dish containing evenly spread photocatalyst powder was subsequently moved into a well-sealed reactor (volume = 0.5 L). The gas composition in the reactor was monitored constantly by the photoacoustic multi-gas monitor. Before each activity evaluation experiment, the photocatalyst was pre-irradiated by introducing pure air (99.9 %) into the reactor and irradiating light from a xenon lamp into the photocatalysts for >12 h to remove any organic contaminant from its surface. A 150-W xenon lamp (HAYASHI-REPIC, LA-410UV-3, 150 W), which was passed through a 422-nm cutoff filter, was employed as the light source for evaluating the photocatalytic activity.

The photoelectrochemical experiment was performed using an electrochemical workstation (Princeton Applied Research, VersaSTAT 3). We prepared the electrode by drop casting method. In detail, we thoroughly grind the photocatalyst in a mortar with ethanol. 20 mg of the ground powder was dispersed in 1 mL ethanol and sonicated for 30 min to form a uniform suspension. The suspension was then drop-casted onto FTO and dried in an oven at 70 °C for 1 h. The electrode was obtained after annealing at 400 °C for 30 min. The photoelectrochemical measurement was carried out using a three-electrode system. The electrolyte is 0.2 M KH₂PO₄ (pH = 7), and the as-prepared electrode served as the working electrode with an illumination area of 1.5 cm². Ag/AgCl and Pt were used as the reference electrode and counter electrode, respectively. Xenon lamp (high power Xenon Light Source, microsolar300 Xe lamp, PerfectLight) equipped with a 450 nm band pass filter was the irradiation light source for the transient photocurrent measurement.

3. Result and Discussion

3.1 First-principles calculations

To investigate the proposed orbital dilution strategy, we calculated the DOS of the pristine and La-doped BiVO₄. Figure 1 and Table 1 reveal the relative position of the VB and CB positions. The energy levels were aligned by comparing the deep-lying O 1s orbitals⁷. The CB positions of pristine and La-doped BiVO₄ were not affected by La doping, whereas VB shifted noticeably as the La doping concentration increased. To evaluate the relationship between the change in the VB position

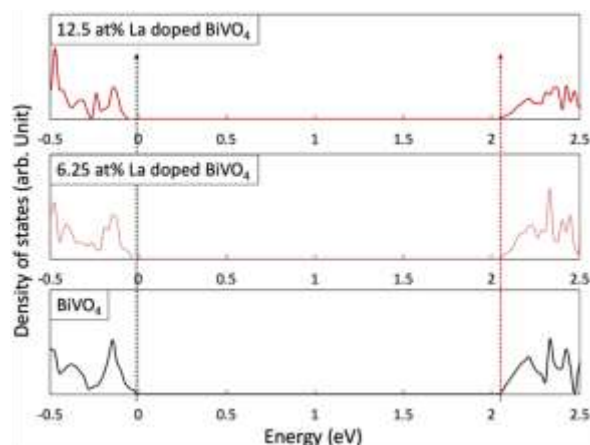


Figure 1 Calculation results of DOS for the La-doped BiVO_4 and pristine BiVO_4 .

and La doping levels, we further investigated the structural change and difference in the orbital hybridization degree caused by La doping. First, the average Bi-to-O bonding distance increased evidently with the increasing doping concentration (SI Note 3, and Table S3). Furthermore, the change in the bonding length could most probably influence Bi *s* and O *p* hybridizations. Thus, we analyzed the hybrid degrees of both orbitals for each structure. Specifically, an electron state, which mainly comprised the Bi *s* and O *p* orbitals, was treated as an indicator of the hybridization degree; a wider width indicated a higher hybridization degree. The enlarged DOS, as well as its width, are shown in Figure S5 and Table S4, respectively (SI). The decreased bandwidth coupled with the increased La doping content indicated the decreased orbital hybridization degrees of the Bi *s* and O *p* orbitals. Further, we compared the DOS intensities of the Bi *s* and O *p* orbitals that were formed at the top of VB. Figure S6 reveals that the continuously decreasing DOS intensity with the increasing La doping content further consolidated the foregoing discussion. The first-principles calculations indicated that bandgap widening could proceed in La- BiVO_4 .

Table 1 Relative CB and VB positions in each structure

	CB (eV)	VB (eV)	Bandgap (eV)
BiVO_4	2.049	-0.029	2.078
6.25 at% La- BiVO_4	2.049	-0.052	2.101
12.5 at% La- BiVO_4	2.049	-0.075	2.124

3.2 Characterization of the synthesized La- BiVO_4

We synthesized La- BiVO_4 , which had been suggested to have a wider gap than its pristine form via simulation, and characterized the crystal structure of each material. As aforementioned, the special VB structure originated from the scheelite monoclinic crystal structure of BiVO_4 . To maintain this structure, the La-doping density was set at <15 at% since phase separation occurred in 20 at% La- BiVO_4 (Figure S7, SI).

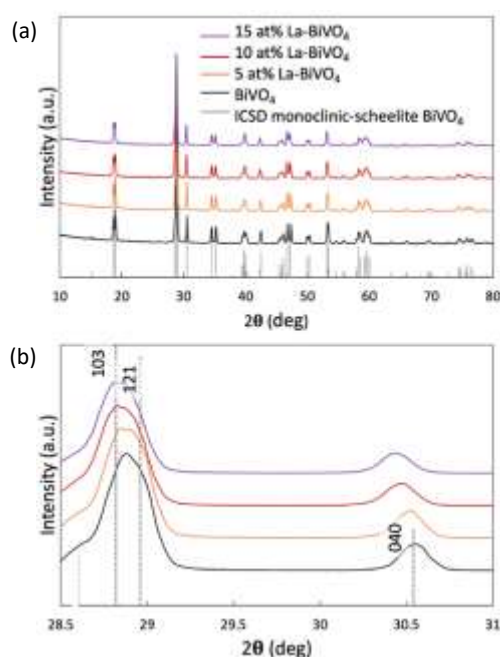


Figure 2 (a) XRD patterns of La- BiVO_4 and pristine BiVO_4 with a standard ICSD pattern of scheelite monoclinic BiVO_4 . (b) Magnified XRD peak patterns

Therefore, we prepared 5, 10, and 15 at% La- BiVO_4 . All of them retained the same crystal structure as that of pristine BiVO_4 (Figure 2(a)). Furthermore, a continuous peak shift was observed in the XRD pattern as the doping level increased (Figure 2 (b)) because the ionic radius of La^{3+} (1.302 Å) was larger than that of Bi^{3+} (1.300 Å)²⁹. The crystallinity of each material was discussed by comparing the intensities of their (121) diffraction peaks (Figure S8). The loss of the diffraction peak intensity indicated the decreased crystallinity of La- BiVO_4 ³⁰. The full width at half maximum (FWHM) revealed that the 10 at% La- BiVO_4 sample exhibited the smallest crystal size (Table S5). Concurrently, we performed the Rietveld analysis of the XRD patterns (SI Note 4, Figures S9 and S10). Table S6 reveals that the lattice constant of the 10 at% La- BiVO_4 was larger than that of pristine BiVO_4 , indicating the same trend as that of the simulation result (Table S2).

Next, the elemental chemical composition and valence states were identified. The EDS elemental mapping results revealed the homogeneous distribution of elemental La in the BiVO_4 crystal (Figure 3(a)). The Bi-to-La ratio in each sample was carefully characterized via ICP-MS. The results revealed that the actual doping amounts were identical to those used in the experimental design (Table S7).

HAXPES was performed to investigate the valence state of each element. Figure 3 shows the results for pristine BiVO_4 and 10 at% La- BiVO_4 , which is the optimum sample for evaluating photocatalytic oxidation activities. The binding energy (BE) value of the La $3d_{5/2}$ orbital (834.95 eV) indicated that the La dopant exhibited a trivalent state in 10 at% La- BiVO_4 ³¹. The BEs of the Bi $4f_{5/2}$, V $2p_{3/2}$, and O $1s$ orbitals were similar before and after lanthanum doping, *i.e.*, trivalent bismuth, pentavalent vanadate, and divalent oxygen anions³¹. Additionally, the broad peak in the O $1s$ spectra at ~533.5 eV was attributed to the chemically adsorbed oxygen on the surface^{32, 33}.

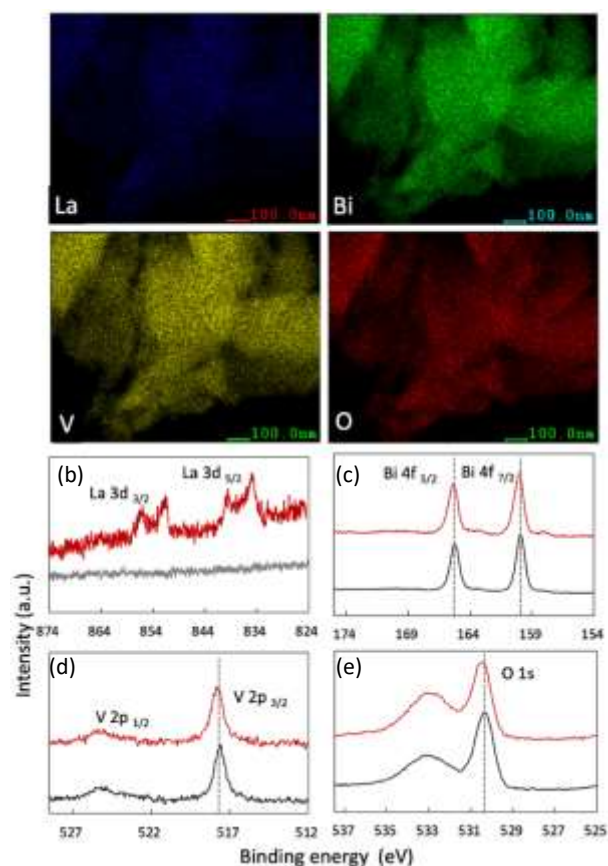


Figure 3 (a) Elemental mapping of 10 at% La-BiVO₄. (b)-(e) HAXPES of each element: 10 at% La-BiVO₄ is represented by the red line, while pristine BiVO₄ is represented by the black line.

Thereafter, we evaluated the optical properties of pristine BiVO₄ and La-BiVO₄. The Tauc plots of each material are shown in Figure 4(a) (their bandgap values are listed in the inset; SI Note 5 contains the calculation details). The bandgap value increased with the increasing La-doping concentration. The corresponding UV-Vis optical absorption spectra are presented in Figure S11 in SI. The PL spectra are shown in Figure S12 in our Supporting Information. Interestingly, the PL spectra of BiVO₄, 5 at% La-BiVO₄, and 10 at% La-BiVO₄ showed a blue-shifted peak, similar to those UV-Vis spectra. However, the PL peak of 15 at% La-BiVO₄ shifted to a longer wavelength. These results suggest that defects are formed in 15 at% La-BiVO₄.

Next, we evaluated the VB top via HAXPES (Figure 4(b)). The VB top positions of 10 at% La-BiVO₄ and pristine BiVO₄ are listed in the inset table of Figure 4(b). The value difference in the VB top position was the same as the bandgap value difference of the pristine BiVO₄ and 10-at% La-BiVO₄, indicating that the bandgap-widening effect was mainly caused by the shift in the position of the VB top. The experimental observations were consistent with our simulation results. Further, our calculation results yielded smaller bandgap values and VB differences than the experimental characterization results because of the inherent shortcomings of the GGA-PBE method, *i.e.*, underestimating bandgap values. Specifically, the bandgap of the shifted VB position was 0.046 eV in the calculation for 12.5

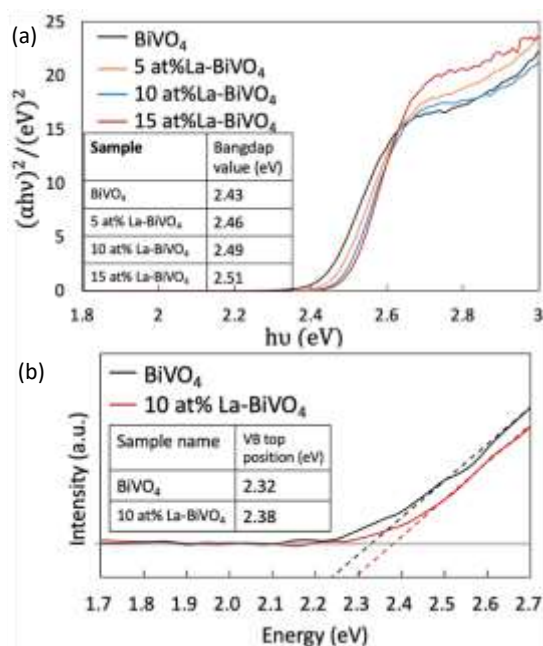


Figure 4 Tauc plots of pristine BiVO₄ and La-BiVO₄. We listed the calculated bandgap value in the inset table. (b) HAXPES of the VB scans of pristine BiVO₄ and 10 at% La-BiVO₄.

at% La-BiVO₄ and 0.06 eV difference for the experimentally synthesized 10 at% La-BiVO₄.

3.3 Photocatalytic oxidation activity

The oxidation reaction of IPA into acetone was selected to evaluate the photocatalytic activity of the photocatalyst. The initial concentration of IPA was set to ~300 ppm, and light from a xenon lamp passing through a 422-nm cut off filter was employed for irradiation during the evaluation (Figure S13). A previous study reported that the concentration of our IPA concentration (this study) and the light intensity followed the light-limited condition in which the photocatalytic activity depended on the number of absorbed photons rather than the diffusion and/or adsorption of the reactants³⁴. Before the evaluation of the photocatalytic activity, the reaction system was set in the dark to allow the reactant to reach an adsorption-desorption equilibrium (the blue region in Figure 5). Afterward, the samples were irradiated with visible light for the evaluation, and we observed superior photocatalytic oxidation performance in the presence of 10 at% La-BiVO₄. Photogenerated holes oxidize the IPA to acetone while photogenerated electrons react with oxygen molecules in air^{34,28}. Possible reaction routes are illustrated in Figure S14.

Here, we calculated the internal QE (IQE) from the photocatalytic evaluation result, which is shown in Figure 5. The IQE value was derived by dividing the rate of the photocatalytic reaction by the absorbed number of photons (the detailed calculation method is described in SI, Note 6). Put differently, the reaction rate was determined by multiplying the number of absorbed photons by IQE. The calculated IQE values and number of absorbed photons for each sample are listed in Table

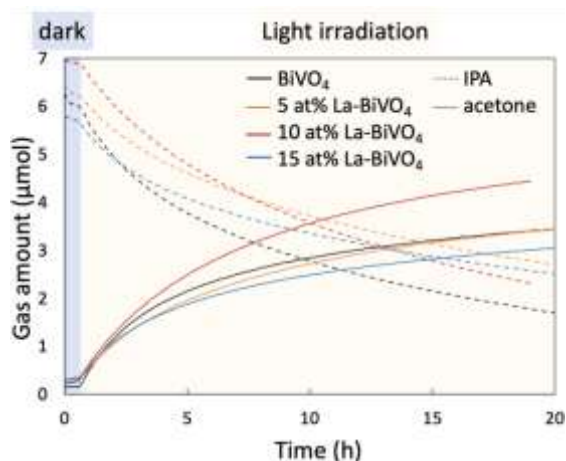


Figure 5 photocatalytic oxidation of IPA into acetone in the presence of pristine BiVO_4 and La-BiVO_4

2. Figure 4 shows that the bandgap-widening effect was observed in the La-BiVO_4 sample; accordingly, the number of absorbed photons under visible light was smaller than that in the presence of pristine BiVO_4 . However, IQE of the 10 at% La-BiVO_4 (4.75×10^{-3} %) was much higher than that of pristine BiVO_4 (3.33×10^{-3} %). Consequently, the photocatalytic activity of 10 at% La-BiVO_4 in the generation of acetone was superior to that of pristine BiVO_4 under the same visible-light-irradiation conditions (Figure 5). Also, the 10 at% La-BiVO_4 is the most active one for water oxidation among all the samples, as displayed in the photocurrent spectra (Figure S15). Although the bandgap of La-BiVO_4 was widened, it was still sensitive to the cyan-light region, which is the strongest in the sunlight spectrum. In addition, the low IQE value of 15 at% La-BiVO_4 arises from defects formed in it, as indicated by the PL spectra (Figure S12).

Table 2 Summary of examined samples' bandgap value, light absorption ability, and internal quantum efficiency.

Sample	Bandgap (eV)	Absorbed photon (mole/second)	Internal quantum efficiency (%)
BiVO_4	2.43	2.78×10^{-6}	3.33×10^{-3}
5 at% La-BiVO_4	2.46	2.43×10^{-6}	3.46×10^{-3}
10 at% La-BiVO_4	2.49	2.36×10^{-6}	4.75×10^{-3}
15 at% La-BiVO_4	2.51	2.27×10^{-6}	3.16×10^{-3}

We carefully analyzed the other properties of the photocatalysts than the VB position, that could affect their catalytic performances. Particularly, we compared the crystallinity, surface area, and gas-adsorption property of each sample since a previous study demonstrated that these parameters could affect the photocatalytic oxidation performance³⁵. Figure S8 shows that 10 at% La-BiVO_4 exhibited lower crystallinity compare to that of pristine BiVO_4 . Generally, low crystallinity inhibits photocatalytic activities; however, the

photocatalytic activity of 10 at% La-BiVO_4 was better than that of the pristine BiVO_4 . We also characterized the gas-adsorption properties of acetone and IPA over pristine BiVO_4 and 10 at% La-BiVO_4 photocatalysts via TG-DTA (Figure S16, Table S9, SI), and no significant difference was observed in their gas-adsorption abilities. Additionally, we evaluated the specific surface areas of the samples via the Brunauer–Emmett–Teller (BET) method (Table S10, SI). Notably, the 10 at% La-BiVO_4 sample exhibited a relatively smaller surface area than the other samples. These results also demonstrate that the improved photocatalytic activity of 10 at% La-BiVO_4 was not simply caused by its surface properties. We suppose that this superior photocatalytic activity and QE are due to the deepened VB of the semiconductor, which exhibited a strong oxidation power. Notably, the bandgap of 10 at% La-BiVO_4 was still narrower than those of TiO_2 and/or WO_3 , and it could absorb the cyan-light region, which is the strongest in the sunlight spectrum.

4. Conclusions

Based on our first-principles calculations, we proposed the orbital dilution strategy for widening the bandgap of narrow-band semiconductors to develop an efficient photocatalyst exhibiting a strong oxidation power. Our calculation results strongly indicated that the doping of La into BiVO_4 could cause a positive shift in VB. Experimentally, we synthesized the La-BiVO_4 samples and confirmed their widened bandgap by doping, as well as the positive shift in their VB positions. The photocatalytic oxidation activities of the undoped BiVO_4 and La-BiVO_4 were evaluated via the oxidation reaction of IPA into acetone conversion reaction. The generation rate of acetone over La-BiVO_4 was higher than that over pristine BiVO_4 . Although the 5 and 10 at% La-BiVO_4 samples exhibited a smaller surface area, lower crystallinity, and lower absorption of photons compared with those of pristine BiVO_4 , their IQEs were superior. This result indicated that the deepened VB position primarily accounted for the improved photocatalytic oxidation performance. The La-BiVO_4 photocatalyst delivered an overall improved oxidation reaction performance. Notably, our La-BiVO_4 with a widened bandgap could still absorb light in the cyan region, which never activates TiO_2 or WO_3 but exhibits the strongest intensity in the sunlight spectrum.

Many previous studies narrowed the bandgaps of wide-gap semiconductors by doping them with impurity ions. However, our study widened the bandgaps of extra narrow-gap semiconductors to boost their photocatalytic activities. As demonstrated by the first-principles calculations and experimental methods, the proposed orbital dilution strategy efficiently tuned the VB position. Our work offers insight into doping-induced bandgap widening for improving photocatalytic performances. Furthermore, we expect that this work would offer insights into the conversion of other inert semiconductors into efficient visible-light-active photocatalysts through bandgap widening.

Author Contributions

Yue Yang conducted the experimental synthesis and first-principles calculations, as well as drafted the manuscript. Dr. Masayuki Toyoda, Dr. Susumu Saito, Mr. Yohei Cho, and Ms. An Niza El Aisnada assisted in the discussions regarding the first-principles calculations. Drs. Hideki Abe and Shigenori Ueda performed HAXPES analysis. Dr. Min Liu assisted in the discussion of photoluminescence and photoelectrochemical measurement results. Mr. Yohei Cho, Dr. Sayuri Okunaka, and Dr. Akira Yamaguchi offered deep insights for discussion. Drs. Hiromasa Tokudome and Masahiro Miyauchi conceived and initiated the project.

The manuscript was written through the contributions of all the authors who have also approved the final version.

Conflicts of interest

There are no conflicts to declare.

Acknowledgements

This work is supported by JST SPRING (Grant No. JPMJSP2106) and JSPS Kakenhi (Grant No. 18H02055) and the International Science and Technology Cooperation Program of China (Grant No. 2017YFE0127800 and 2018YFE0203400). We thank Dr. Yuichiro Matsushita of the Tokyo Institute of Technology for his assistance with the first-principles calculations. We appreciate the Tokyo Tech Academy for Convergence of Materials and Informatics (TAC-MI) for facilitating the communication between physical-theory and materials-engineering researchers, as well as for ensuring that we conducted a thorough investigation. We appreciate Dr. Ryo Ohta at the Material Analysis Division of the Open Facility Center (Tokyo Institute of Technology) for the ICP-MS analysis. The HAXPES measurements were conducted with the approval of the NIMS Synchrotron X-ray Station (Proposals 2020A4600 and 2020A4650).

Notes and references

- 1 A. Fujishima and K. Honda, *Nature*, 1972, **238**, 37–38.
- 2 R. Asahi, *Science*, 2001, **293**, 269–271.
- 3 H. Kato and A. Kudo, *J. Phys. Chem. B*, 2002, **106**, 5029–5034.
- 4 R. Abe, K. Hara, K. Sayama, K. Domen and H. Arakawa, *Journal of Photochemistry and Photobiology A: Chemistry*, 2000, **137**, 63–69.
- 5 J. Tang, A. J. Cowan, J. R. Durrant and D. R. Klug, *J. Phys. Chem. C*, 2011, **115**, 3143–3150.
- 6 J. Liu, Y. Liu, N. Liu, Y. Han, X. Zhang, H. Huang, Y. Lifshitz, S.-T. Lee, J. Zhong and Z. Kang, *Science*, 2015, **347**, 970–974.
- 7 W. J. Jo, H. J. Kang, K.-J. Kong, Y. S. Lee, H. Park, Y. Lee, T. Buonassisi, K. K. Gleason and J. S. Lee, *Proceedings of the National Academy of Sciences*, 2015, **112**, 13774–13778.
- 8 L. Yu, X. Ba, M. Qiu, Y. Li, L. Shuai, W. Zhang, Z. Ren and Y. Yu, *Nano Energy*, 2019, **60**, 576–582.
- 9 J. Kim, C. W. Lee and W. Choi, *Environmental Science & Technology*, 2010, **44**, 6849–6854.
- 10 H. Yu, H. Irie, Y. Shimodaira, Y. Hosogi, Y. Kuroda, M. Miyauchi and K. Hashimoto, *The Journal of Physical Chemistry C*, 2010, **114**, 16481–16487.
- 11 A. Kudo, K. Omori and H. Kato, *Journal of the American Chemical Society*, 1999, **121**, 11459–11467.
- 12 D. J. Payne, M. D. M. Robinson, R. G. Egdell, A. Walsh, J. McNulty, K. E. Smith and L. F. J. Piper, *Appl. Phys. Lett.*, 2011, **98**, 212110.
- 13 A. Walsh, D. J. Payne, R. G. Egdell and G. W. Watson, *Chem. Soc. Rev.*, 2011, **40**, 4455.
- 14 G. V. Govindaraju, J. M. Morbec, G. A. Galli and K.-S. Choi, *J. Phys. Chem. C*, 2018, **122**, 19416–19424.
- 15 Z. Jin, Y. Zhang, D. Liu, H. Ding, B. B. Mamba, A. T. Kuvarega and J. Gui, *Separation and Purification Technology*, 2021, **277**, 119224.
- 16 M. Miyauchi, M. Takashio and H. Tobimatsu, *Langmuir*, 2004, **20**, 232–236.
- 17 G. Kresse and J. Hafner, *Phys. Rev. B*, 1993, **47**, 558–561.
- 18 G. Kresse and J. Hafner, *Phys. Rev. B*, 1994, **49**, 14251–14269.
- 19 G. Kresse and J. Furthmüller, *Phys. Rev. B*, 1996, **54**, 11169–11186.
- 20 G. Kresse and J. Furthmüller, *Computational Materials Science*, 1996, **6**, 15–50.
- 21 P. E. Blöchl, *Phys. Rev. B*, 1994, **50**, 17953–17979.
- 22 G. Kresse and D. Joubert, *Phys. Rev. B*, 1999, **59**, 1758–1775.
- 23 J. P. Perdew, K. Burke and M. Ernzerhof, *Phys. Rev. Lett.*, 1997, **78**, 1396–1396.
- 24 J. P. Perdew, K. Burke and M. Ernzerhof, *Phys. Rev. Lett.*, 1996, **77**, 3865–3868.
- 25 A. W. Sleight, H.-y. Chen, A. Ferretti and D. E. Cox, *Materials Research Bulletin*, 1979, **14**, 1571–1581.
- 26 M. J. Puska, S. Pöykkö, M. Pesola and R. M. Nieminen, *Phys. Rev. B*, 1998, **58**, 1318–1325.
- 27 S. Bernal, J. A. Daz, R. Garcia and J. M. Rodriguez-Izquierdo, *Journal of Materials Science*, 1985, **20**, 537–541.
- 28 F. Arzac, D. Bianchi, J. M. Chovelon, C. Ferronato and J. M. Herrmann, *The Journal of Physical Chemistry A*, 2006, **110**, 4202–4212.
- 29 R. Li, Z. Qu and J. Fang, *Physica B: Condensed Matter*, 2011, **406**, 1312–1316.
- 30 W. Ruland, *Acta Cryst*, 1961, **14**, 1180–1185.
- 31 J. F. Moulder and J. Chastain, *Handbook of X-ray Photoelectron Spectroscopy: A Reference Book of Standard Spectra for Identification and Interpretation of XPS Data*, Physical Electronics Division, Perkin-Elmer Corporation, 1992.
- 32 J.-C. Dupin, D. Gonbeau, P. Vinatier and A. Levasseur, *Physical Chemistry Chemical Physics*, 2000, **2**, 1319–1324.
- 33 L. Q. Wu, Y. C. Li, S. Q. Li, Z. Z. Li, G. D. Tang, W. H. Qi, L. C. Xue, X. S. Ge and L. L. Ding, *AIP Advances*, 2015, **5**, 097210.
- 34 Y. Ohko, K. Hashimoto and A. Fujishima, *The Journal of Physical Chemistry A*, 1997, **101**, 8057–8062.
- 35 G. Tian, H. Fu, L. Jing and C. Tian, *Journal of Hazardous Materials*, 2009, **161**, 1122–1130.